J Sign Process Syst (2009) 55:103–112
DOI 10.1007/s11265-008-0179-5

Detection of Retinal Blood Vessels Based on Nonlinear Projections

Yongping Zhang · Wynne Hsu · Mong Li Lee

Received: 13 November 2007 / Accepted: 3 April 2008 / Published online: 17 June 2008

Abstract An automated method for blood vessel segmentation is presented in this paper. The approach uses the nonlinear orthogonal projection to capture the features of vessel networks, and derives a novel local adaptive thresholding algorithm for vessel detection. By embedding in a kind of image decomposition model, the selection of system parameter which reflects the size of concerned convex set is examined. This approach differs from previously known methods in that it uses matched filtering, vessel tracking or supervised methods. The algorithm was tested on two publicly available databases: the DRIVE and the STARE. By comparison with hand-labeled ground truth, an average accuracy of 96.1% is achieved on the former database, and an average accuracy of 90.8% is achieved on the later database.

Keywords Retinal imaging · Vessel detection · Nonlinear orthogonal projection · Image decomposition · Adaptive thresholding · Parameter selection

Y. Zhang
School of Electronic and Information Engineering,
Ningbo University of Technology,
Cuibai Road,
Ningbo 315016, China

Y. Zhang (✉) · W. Hsu · M. L. Lee
Department of Computer Science,
National University of Singapore,
3 Science Drive 2,
Singapore 117543, Singapore
e-mail: zhangyp1963@yahoo.com

W. Hsu
e-mail: whsu@comp.nus.edu.sg

M. L. Lee
e-mail: leeml@comp.nus.edu.sg

1 Introduction

The quantitative analysis of vessels and optic disk appearances on scanning retinal images forms an essential step in solving diagnosis problem of some eye diseases, such as diabetic retinopathy (DR) [1–3], glaucoma [4, 5], and myopia [6, 7]. The convenient manual measurements through visual inspection, however, can become time-consuming, tedious or even impossible when the vascular network is complex, or the signal-to-noise is weak. Therefore, developing a tool to automate the process of analysis is a feasible solution to overcome the disadvantages of visual analysis.

The application of image processing and pattern recognition techniques to the diagnosis of retinal disease is rapidly becoming a reality due to the broad-based acceptance of electronic imaging devices throughout the medical community and through the collection and accumulation of large patient histories in picture archiving and communications systems. The employment of digital imaging in ocular anatomy and pathology provides us with digitized data that could be exploited for computerized detection of eye disease.

Automated approaches to blood vessel delineation in scanning retinal images can be roughly divided into two main categories: synchronous network segmentation and single vessel tracking. The former class synchronously classifies each pixel based on some local features, including matched filtering (e.g., [8, 9]), edge-based method (e.g., [10, 11]), local adaptive thresholding (e.g., [12]), wavelet transform [2, 13] and morphological filtering [14, 15]. The tracking methods search a continuous vessel segment starting from a point given by manually or automatically, based on certain local properties [3, 16–19]. For instance, in [16] the local gray-level minimum was used as a criterion to search the link point; in [17] the fuzzy *C*-means clustering algorithm was applied to estimation of next search location; a Kalman filter was employed to perform vessel pixel tracking in [18]; while in [3] and [19] the parameters of Gaussians were estimated for modeling the vessel intensity profiles. Beyond these, the work in [20] combines principal component analysis with neural network to classify image pixels, while [21] employs the feature vectors from ridge extraction and the kNN-classifier for vessel detection.

In this paper, we present a novel method for vessel network segmentation in the basis of nonlinear projections [24]. The input image (inverted green channel of scanned retinal image) is firstly projected onto a closed convex set consisting of functions with zero mean, and then the signs of the projection are regarded as the outputs of the proposed segmentation system.

Nonlinear projection algorithm has been introduced to solve total variation minimization problems involved in image decompositions [24, 29]. In general, an image may contain geometrical information and texture information. The goal of image decompositions is to split an original image into two components: one stands for the structural part and one stands for the textural part. Such a decomposition problem can be modeled by convex optimization scheme [22–26]. The fundamental idea of the nonlinear projection algorithm is to transform the original convex optimization problem into searching the projection of the given image function into a bounded convex ball of a Banach space, G space [26, 31]. The G space is composed of oscillating functions in the means of having zero mean.

In the present study, the oscillating components of scanning retinal images are adopted to capture the features of blood vessel networks. Furthermore, a vessel detection algorithm is derived from the nonlinear projections. This is a new adaptive thresholding method compared with the variational image binarization algorithm introduced in [32]. Both methods perform automatic thresholding with threshold surfaces generated by using variational models.

In order to improve the segmentation results, morphological open operations are also applied for post processing of resulting binary images. Finally, the images from two publicly available databases, the DRIVE database [21] and the STARE database [8], are used to evaluate the method proposed.

The remainder of this paper is organized as follows. In Section 2, we describe the fixed point algorithm for estimating the nonlinear orthogonal projection of an image function onto a bounded closed convex set that consists of oscillating functions. We also discuss the problem of determining an optimal radius of the closed convex set. In Section 3, we detail the vessel detection algorithm. In Section 4, we present the evaluation of results. Finally, we conclude the paper in Section 5.

2 Nonlinear Projections

As well-known, to deeply understand the properties of a function, such as temporal signals or spatial signals, one can project the function onto different subspaces consisting

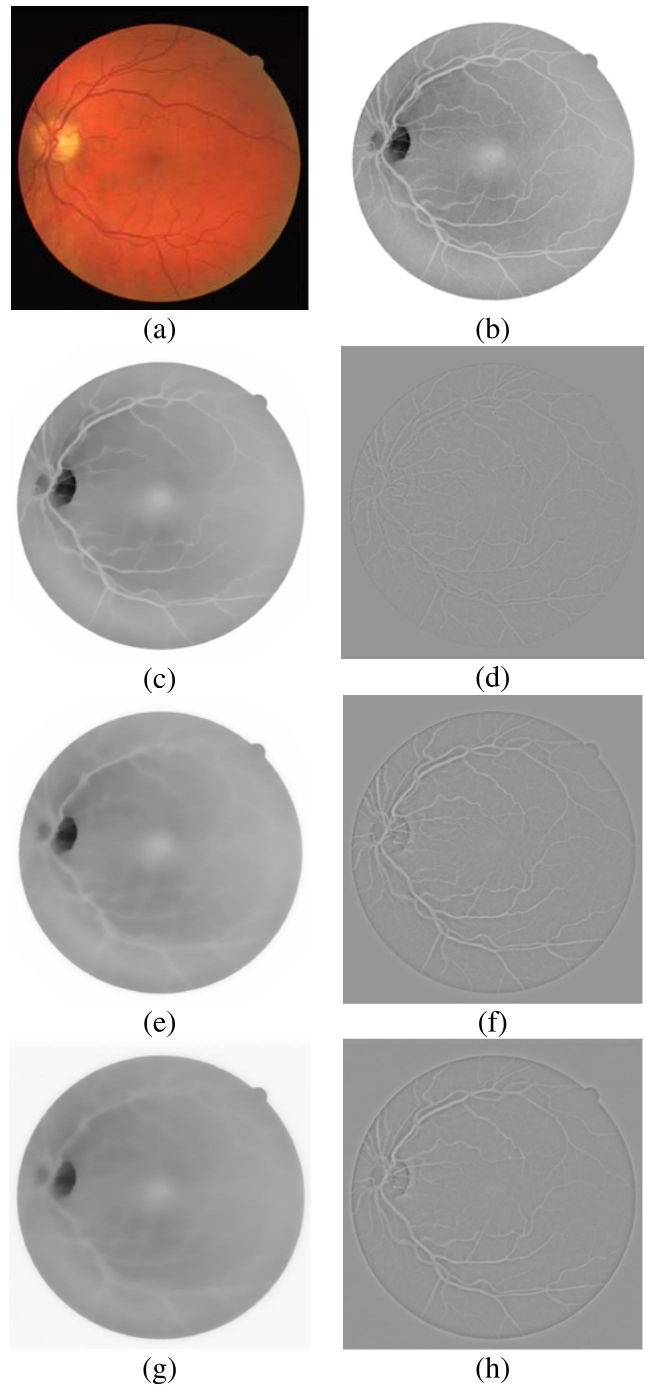

Figure 1 Results of decomposition with varying parameter μ. **a** Original retinal image from DRIVE database. **b** Inverted green channel severed as input. **c** and **d** are the resultant bounded variation component u and oscillating component μ+150 using μ=15. **e** and **f** are the resultant bounded variation component u and oscillating component v+150 using μ=65. **g** and **h** are the resultant bounded variation component u and oscillating component v+150 using μ=85μ.

of special functions, and then obtain the representation of the function. Fourier transforms and wavelet transforms are the typical examples. In the past decade, a kind of variational methods, total variation minimization, has been applied to the representation of two dimensional images [22–31]. In this section, we will recall some basic facts about nonlinear projections onto closed convex sets and variation-based image decompositions. A fixed point algorithm for computing the nonlinear projection and a method for determining the radius of a closed convex set which serves as a projective space will also be presented.

2.1 Projection onto a Convex Set

Let H be a Hilbert space, $X \subset H$ be convex, closed, and non-empty. Recall that for $g \in H$, we defined $P_x g$, called the projection of g onto X, to be the optimum for

$$\min_{v\in X}\frac{1}{2}\|g-v\|^2. \tag{1}$$

That is, the minimizer is the closest point in X to g. An interesting property of the projection function is that for any $g \in H$ there is a unique optimum for Eq. 1.

From now on, we consider the discrete case, two dimensional digital images. All the functions will be 2-dimensional matrices of size $M \times N$. A digital image may include both structural information and textural information. The structural part can be considered as the function with bounded variation, and the textural or noise part can be considered as oscillating function with zero mean [22–26]. In order to capture the texture information, we will consider the projection onto a closed convex set consisted of oscillating functions.

Let X_0 be the space of functions with zero mean:

$$X_0 = \left\{ v : \sum_{i,j} v_{i,j} = 0 \right\}. \tag{2}$$

It was proven that the set X_0 identifies with the following set of functions [25]:

$$G = \{v : \exists \xi = (\xi_1, \xi_2) \in L^\infty \times L^\infty, s.t. \quad v = div\xi\}, \tag{3}$$

where div represents the divergence of a vector-valued function $\mathrm{div}\xi = \partial\xi_1/\partial x + \partial\xi_2/\partial y$. On G, a Banach norm, so-called G norm, is defined as [26, 31]:

$$\|v\|_G = \inf\left\{ \|\xi\|_\infty : v = div\xi, |\xi_{i,j}| = \sqrt{(\xi_1)_{i,j}^2 + (\xi_2)_{i,j}^2} \right\}, \tag{4}$$

where $\|\xi\|_\infty = \max_{i,j}|\xi_{i,j}|$. The set G with the corresponding G norm defined in Eq. 4 is called G space.

To get the textural part of an image f, a natural idea is to project the original image into a bounded subset of space G.

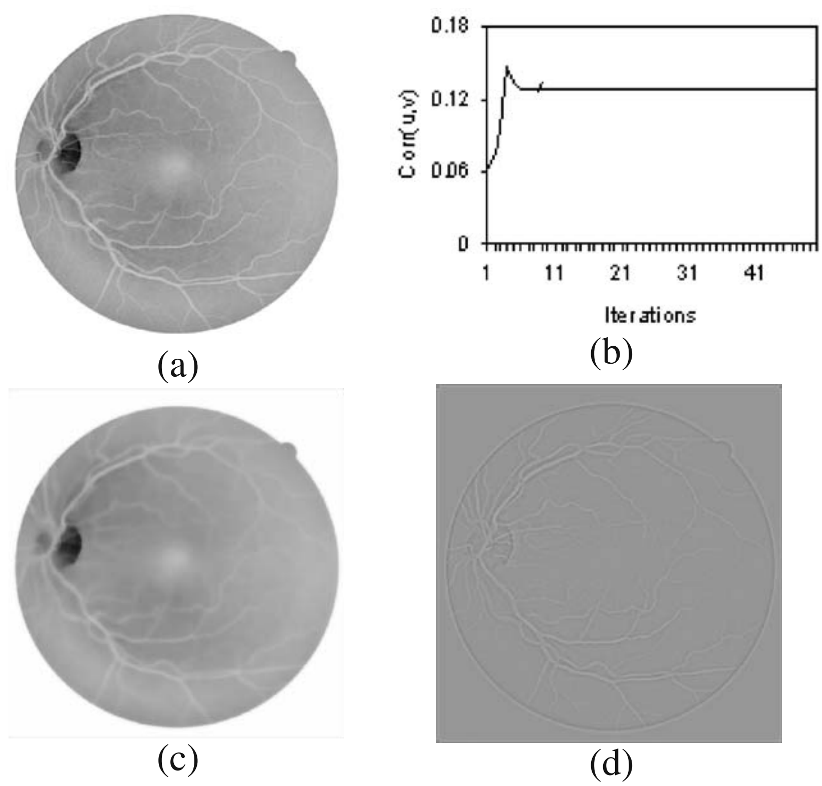

Figure 2 An example for parameter selection. **a** Input image shown in Fig. 1b. **b** Correlation graph. **c** and **d** are the corresponding components u and $v+150$ using a better value of μ=40.

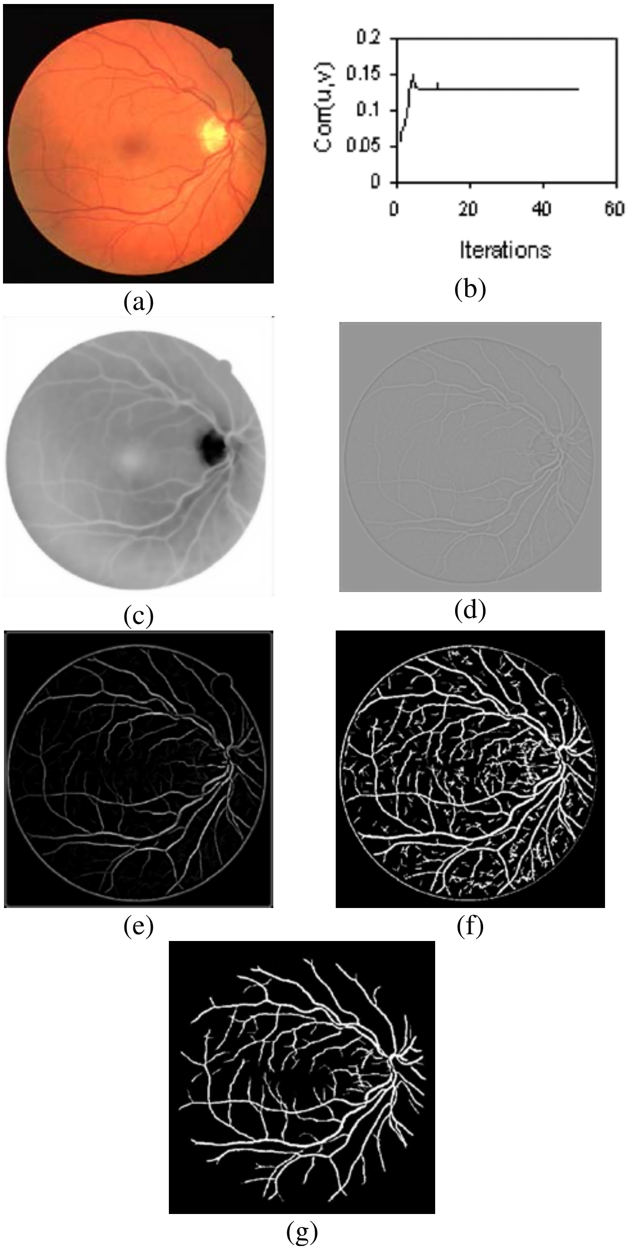

Figure 3 Example for an image in the DRIVE set. **a** Original image from DRIVE database. **b** Correlation graph. **c** and **d** are the corresponding components u and v+150 using a better value of μ= 40. **e** Positive part of v, where the values of v_+ are converted by $(v_+)_{i,j} \rightarrow 255 * (v_+)_{i,j} / .\max(v_+)$. **f** Automatically thresholding result using formula 12. **g** Final segmentation result by using open operation and image filed masking.

For a non-negative constant μ, if we denote by G_μ the closed ball with radius μ:

$$G_\mu = \{v : v \in G, \|v\|_G \leq \mu\}, \tag{5}$$

then G_μ is a closed convex subset of G.

The existing approaches have revealed that the projection $P_{G_\mu} f$ can perceive the scales of objects in the image f via adjusting the value of parameter μ [27, 28]. That is, by changing the value of μ, we can perform a multiscale analysis for the given image. In the next subsection, we will describe a fixed point algorithm for computing the projection $P_{G_\mu} f$.

2.2 Fixed Point Algorithm

Computing the projection $P_{G_\mu} f$ amounts to finding the solution of the following problem:

$$\min\left\{ \|\mu \mathrm{div}\xi - f\|_{L^2}^2 : \max_{i,j} |\xi_{i,j}| \leq 1 \right\}. \tag{6}$$

This problem can be solved by a fixed point algorithm: ξ^0=0, and

$$\xi_{i,j}^{n+1} = \frac{\xi_{i,j}^n + \tau(\nabla(\mathrm{div}\xi^n - f/\mu))_{i,j}}{1 + \tau\left|(\nabla(\mathrm{div}\xi^n - f/\mu))_{i,j}\right|}. \tag{7}$$

It was proven that if $\tau \leq 1/8$, then $\mu div\xi^n$ converges to $P_{G_\mu} f$ as $n \rightarrow \infty$ [24].

In the past years, a popular variation model, so-called ROF model, has been applied for decomposing an image $f \in L^2(\Re^2)$ into a sum of two functions μ+v, where $\mu \in BV(\Re^2)$ is a function of bounded variation, while $v \in L^2(\Re^2)$is an oscillating function representing texture

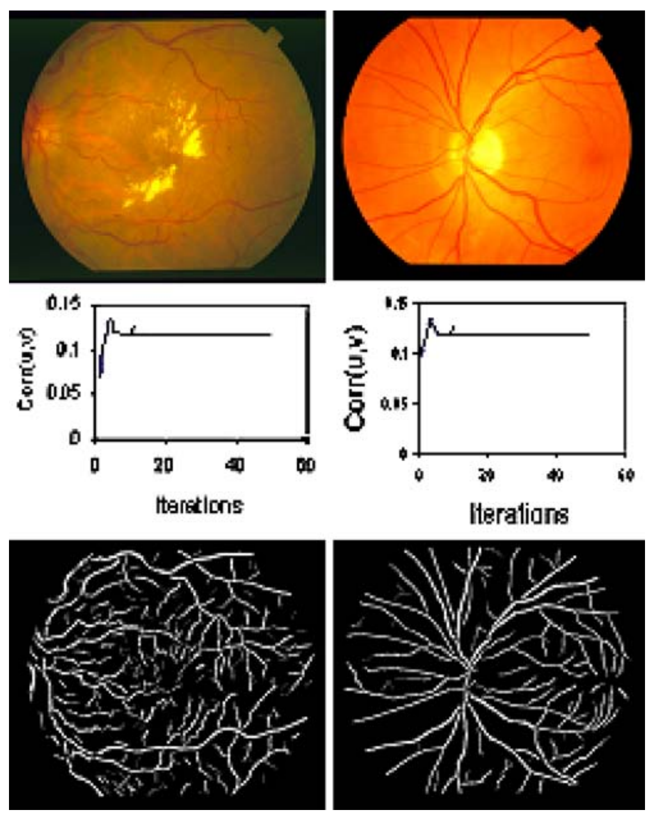

Figure 4 Example for two images in the STARE set. *Top row* Original images from the STARE database. *Middle row* Correlation graphics. *Bottom row* Vessel detection results.

or noise [22–26]. The decomposition problem can be modeled by the following total variation minimization:

$$\min_{(u,v)\in BV\times L^2/f=u+v}\left(\int|\nabla\mu|+\frac{\int v^2}{2\mu}\right) \tag{8}$$

where $\int|\nabla\mu|$ is the total variation of u, $\mu>0$ is the regularization parameter, serving as a scaling level to separate the two terms. If we let $v=P_{G_\mu}f$, and $\mu=f-P_{G_\mu}f$, then it was proven that u and v are the solution of Eq. 8 from standard convex duality theory [24]. From the notation above, we can see that for a given constant μ the projection procedure can be embedded into a decomposition procedure. In the next subsection, we will utilize this embedding to address the selection problem of the radius μ.

2.3 Radius Selection

The parameter μ determines the size of the convex ball G_μ and hence the property of the corresponding nonlinear projective. In the image decomposition model 8, μ serves as a regularization parameter to balance the bounded variation

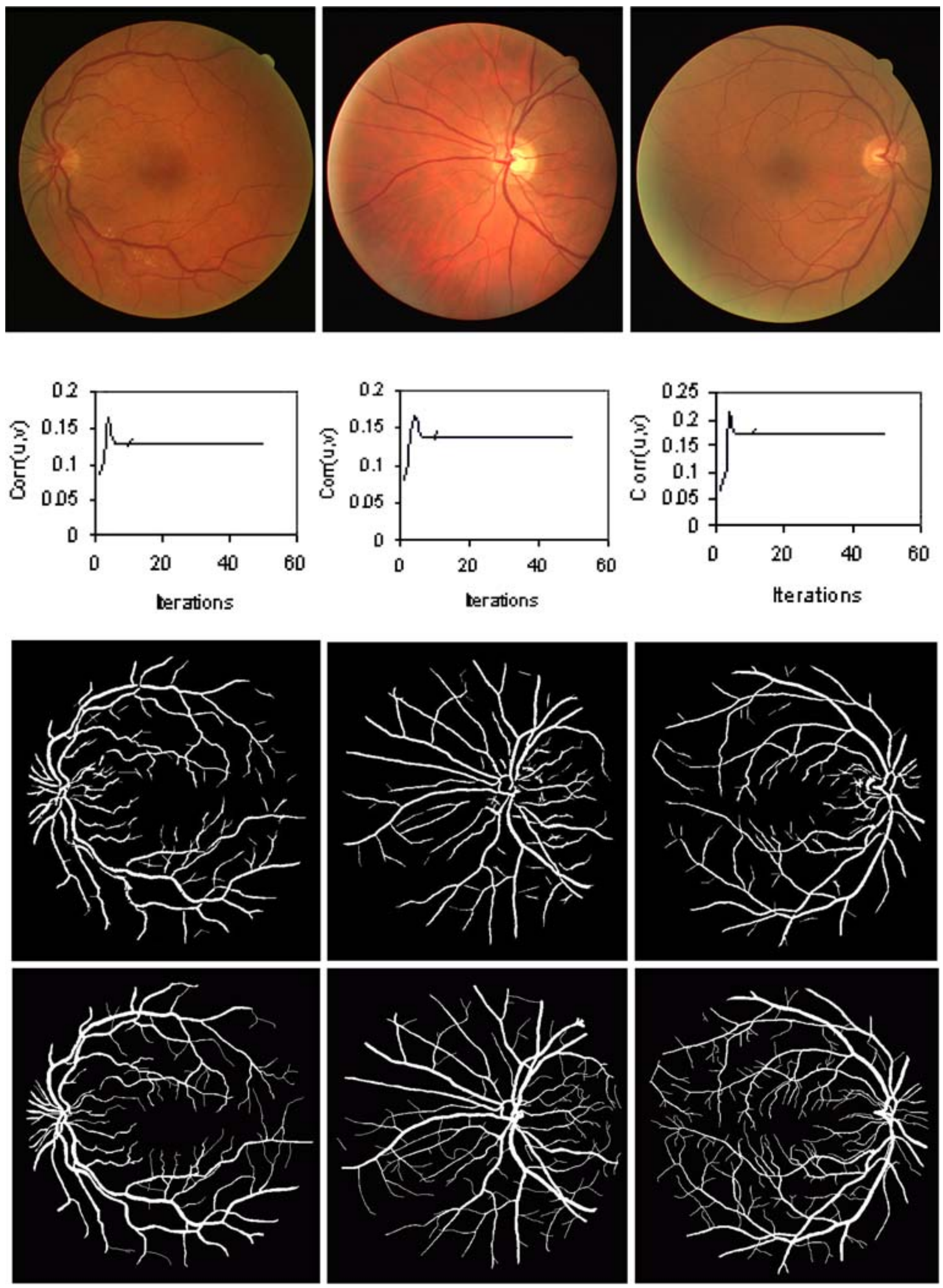

Figure 5 Vessel segmentation on images from the DRIVE database. *First row* original images. *Second row* Correlation graphs of the orthogonal projective and the bounded variation components. *Third row* segmented images using our method. *Last row* manual labeled results from DRIVE database (first human observer) [21].

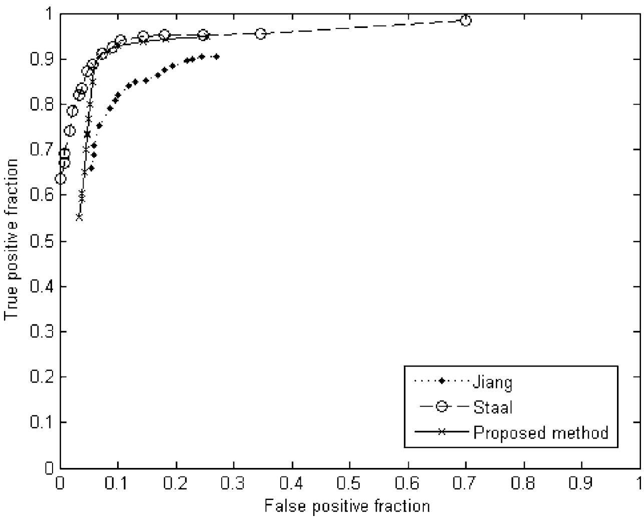

Figure 6 Average performance over 40 images from the DRIVE database: our approach vs. the approaches reported in [12] and [21].

and the oscillating components. As illustrated in Fig. 1, larger values of μ result in the bounded variation components being smoother and the oscillating component including more details or small textured patterns. If μ is chosen too large, however, then only a over-smoothed structure of the original image is kept in the bounded variation component, while some features with larger scale will be swept into the oscillating component. The parameter μ must be adaptively chosen with varying images for obtaining satisfactory effects.

In practice, there were some approaches for selection of regularization parameter, including adaptive iteration method [22, 24], scale related automatic method [28] and correlation graph-based selection method [29]. In this study, we employ the correlation between the bounded variation and oscillating components as a measure to select optimal parameter. The correlation between $\mu = f - P_{G_\mu} f$ and $v = P_{G_\mu} f$ is defined as:

$$\mathrm{corr}(u, v) = \frac{\mathrm{cov}(\mathrm{u}, \mathrm{v})}{\sigma_u^2 \sigma_v^2}, \tag{9}$$

where σ_g^2 represents the variance of function g, $cov(g, h)$ represents the covariance between functions g and h defined as:

$$\mathrm{cov}(\mathrm{g}, \mathrm{h}) = \frac{1}{\mathrm{M} \times \mathrm{N}} \sum_{\mathrm{i,j}} \left(\mathrm{g_{i,j}} - \bar{g}\right)\left(\mathrm{h_{i,j}} - \bar{h}\right). \tag{10}$$

It is easy to see that

$$|corr(u, v)| \leq 1. \tag{11}$$

The ideal decomposition result should be that the two components are not correlated, that is, $\mathrm{corr}(u, v) = 0$. As proved in [28], $\mathrm{corr}(u, v) \geq 0$ holds for any positive μ. Hence

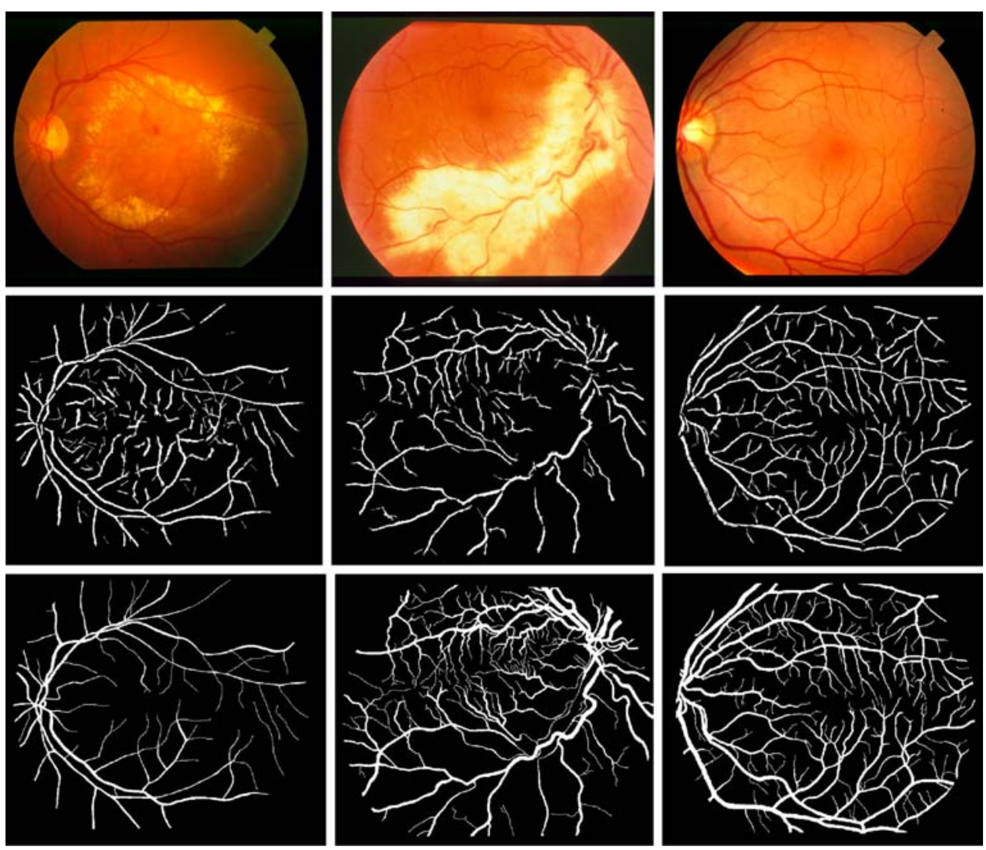

Figure 7 Vessel segmentation on images from the STARE database. *Top row* original images. *Middle row* segmented images using our method. *Bottom row* manual labeled results from STARE database (second human observer) [8].

we can select an optimal parameter μ based on minimizing the correlation. Figure 2 shows an example, where the input image is the inverted green channel of image of Fig. 1a. The correlation $\mathrm{corr}(u, v)$ of 50 values of μ is plotted. The initial value of μ was set as μ^0=4, and each time the value of μ was set as $\mu^n = 4 \cdot (n+1)$. After 50 iterations, a better value of μ^0=40 (corresponding to n=9) was found.

3 Vessel Detection Algorithm

3.1 Algorithm Description

From the notations above, the nonlinear projection can be used to capture the texture structures in images. In this approach, we employ the orthogonal projection to perform retinal blood vessel detection.

Motivated by the identical relationship between G and X_0, we get an automatic method to threshold the projective as:

$$\mathrm{Out}_{i,j} = \begin{cases} 1, & \left(P_{G_\mu} f\right)_{i,j} > 0 \\ 0, & \text{otherwise} \end{cases}. \tag{12}$$

This is equivalent to the global thresholding using the mean of projective as a threshold value, because $P_{G_\mu} f$ belongs to the set X_0. From the decomposition model 8 and the notations, the method is also equivalent to the following local adaptive thresholding with threshold surface u:

$$\mathrm{Out}_{i,j} = \begin{cases} 1, & f_{i,j} > u_{i,j} \\ 0, & \text{otherwise} \end{cases}, \tag{13}$$

since $P_{G_\mu} f = f - \mu$. In some means, this is a new variational image binarization algorithm in comparison with the method proposed in [32], where a multiscale variation model was introduced to generate smooth threshold surface.

After thresholding the projective, the morphological open operators are applied for removing blob-like structures and some shorter linear structures in the resulting binary image. In the experiments of this approach, the open operators with linear structural elements are applied to the binary image along twelve directions (0°, 15°, 30°, …, and 165°). The length of linear structure elements is set as 17 pixels. Our vessel detection algorithm can be summarized as the following steps:

Step 1. Choose a parameter μ, compute the orthogonal projective $P_{G_\mu} f$ using the fixed point algorithm 7.

Step 2. Threshold the projective as stating in Eq. 9 to get the output binary image Out.

Step 3. Apply morphological open operators to the binary image Out to remove blob-like structures and some shorter linear structures.

3.2 Examples

In this subsection, we present two examples working on the DRIVE and the STARE databases to illustrate our method.

Example 1 An image from the test set of DRIVE database [21]. In the experiment, the inverted green component serves as input image; the optimal parameter μ=40, the first local minimum of the correlation function, is reached by nine iterations; the positive part $\left(P_{G_\mu} f\right)$+of $P_{G_\mu} f$ is shown in Fig. 3e. For a function g, its positive part is defined as:

$$(g_+)_{i,j} = \begin{cases} g_{i,j}, & g_{i,j} \geq 0 \\ 0, & \text{otherwise} \end{cases}. \tag{14}$$

The automatically thresholding result using formula 12 is shown in Fig. 3f. By using image field of view masking with the mask from the DRIVE database and morphological open filtering, the final segmentation result is presented in Fig. 3g.

Example 2 Two images from the STARE database. One is for normal case and another one is for abnormal case. The processing results are shown in Fig. 4. As can be seen from the results, the parameter μ also reaches to the first local minimum μ=40 by nine iterations on the two images.

4 Experimental Results

In order to evaluate the performance of proposed method, three measures, including false positive fraction (FPF) which represents the fraction of pixels erroneously detected as vessel pixels, true positive fraction (TPF) which represents the fraction of pixels correctly detected as vessel

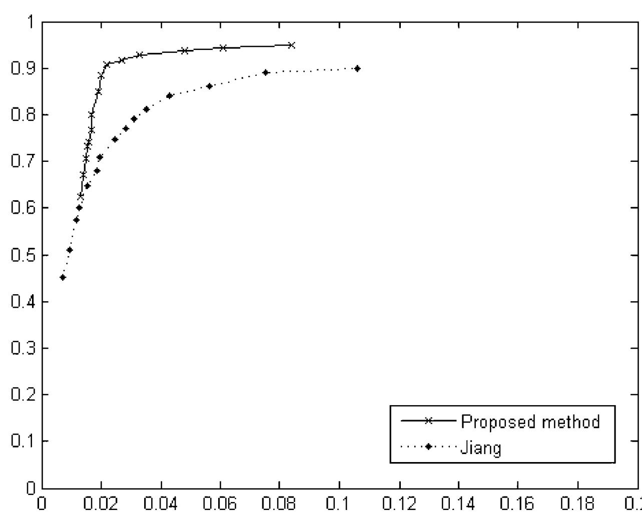

Figure 8 Average performance over 20 images from the STARE database: our approach vs. the method reported in [12].

pixels, and average accuracy (AA) which represents the ratio of the total number of correctly classified pixels (both of true positive and true negative) by the number of pixels in the image filed are employed. These measures are defined as follows:

$$\mathrm{FPF} = \frac{\#\mathrm{pixels\_erroneously\_detected\_as\_vessel\_pixels}}{\#\mathrm{pixels\_are\_actually\_in\_background}}, \tag{15}$$

$$\mathrm{TPF} = \frac{\#\mathrm{pixels\_correctly\_detected\_as\_vessel\_pixels}}{\#\mathrm{Pixels\_are\_actually\_in\_vessels}}, \tag{16}$$

$$\mathrm{AA} = \frac{\#\mathrm{pixels\_correctly\_detected\_as\_bachground\_or\_vessel\_pixels}}{\#\mathrm{pixels\_in\_the\_whole\_image\_field}}. \tag{17}$$

Obtaining large databases with ground truth is essential in developing effective systems for vessel detection that can be used in retinal image analysis. However, this is difficult to achieve as the ground truth generation is a tedious process that demands patience. In the course of our approach, two publicly available datasets, DRIVE and STARE which include both the original images and the corresponding ground truth markings are used. In order to benchmark against the reported methods, the 40 images from both the test and training set of DRIVE database [21] and the 20 images from the website of STARE project [8] were used for evaluating our detection method. By examining the total of 60 images, the value of μ=40 can be employed as a common optimal parameter for computing the nonlinear projection of images from both databases.

Images from DRIVE database [21] The total 40 images from both the test and training set of DRIVE database [21] were used. As shown in Fig. 5, the detection results using our method and the manual labeled results (first set) from DRIVE database are compared. Using the manual labeled set as a reference, the TPF, the FPF and the average accuracy are 0.754%, 0.0228% and 96.1%, respectively. For comparison purpose, the corresponding average performance curves (the plotting of TPF against FPF) of the methods reported in the present, the literature [12] and the literature [21], are shown in Fig. 6.

Images from STARE database [8] Figure 7 illustrates the segmentation results on three images from the STARE database. Where the manual labeled results is downloaded from the website of STARE project [8] (http://www.parl.clemson.edu/stare/probing/). For the total of 20 images, where half is normal and half is abnormal, the TPF, the FPF and the average accuracy are 0.9373%, 0.0264% and 90.87%, respectively. The average performance curve over the 20 images is shown in Fig. 8 for the present approach and the method reported in [12].

5 Conclusions

The nonlinear projection algorithm has been recently applied to image processing and analysis [24, 29]. However, to our knowledge, there have been no published reports on the applications of nonlinear projections to retinal image analysis. In this paper, we have proposed a new approach to the automatic detection of retinal blood vessels based on nonlinear projections. The approach involved in selecting an optimal radius of the bounded convex set of oscillating functions. The radius can be also considered as the regularization parameter of ROF's image decomposition model [22]. The experimental results indicate that to all the used images there is a common suited parameter for the procedure of nonlinear projection and more than 96 percent of pixels have been correctly classified for the images from the DRIVE and the STARE databases.

Acknowledgements The authors would like to thank the anonymous reviewers for their comments and suggestions which have greatly improved the presentation of this paper. The authors also thank the authors of DRIVE and STARE databases for making their databases publicly available.

References

1. Kahai, P., Namuduri, K. R., & Thompson, H. (2006). A decision support framework for automated screening of diabetic retinopathy. *Inernational Journal of Biomedical Imaging,* 1–8.
2. Cornforth, D. J., Jelinek, H. J., Leandro, J. J. G., Soares, J. V. B., Cesar, R. M. Jr., et al. (2004). Development of retinal blood vessel segmentation methodology using wavelet transforms assessment of diabetic retinopathy, *The 8th Asia Pacific Symposium on Intelligent and Evolutionary Systems*, 50–60.
3. Li, H., Hsu, W., Lee, M. L., & Wang, H. (2005). Automatic grading of retinal vessel calibre. *IEEE Transactions on Biomedical Engineering*, *52*(7), 1352–1355.
4. Broadway, D. C., Drance, S. M., Parfitt, C. M., & Mikelberg, F. S. (1998). The ability of scanning laser ophthalmoscopy to identify various glaucomatous optic disk appearances. *American journal of ophthalmology*, *125*(5), 593–604.
5. Miglior, S., Guareschi, M., Albe', E., Gomarasca, S., Vavassori, M., & Orzalesi, N. (2003). Detection of glaucomatous visual field changes using the moorfields regression analysis of the Heidelberg retina tomograph. *American Journal of Ophthalmology*, *136*(1), 26–33.
6. Vongphanit, J., Michell, P., & Wang, J. J. (2002). Population prevalence of titled optic disks and the relationship of this sign to refractive error. *American Journal of Ophthalmology*, *133*(5), 679–685.

7. Vongphanit, J., Michell, P., & Wang, J. J. (2002). Prevalence and progression of myopic retinopathy in an older population. *Ophthalmology*, *109*, 704–711.
8. Hoover, A., Kouznetsova, V., & Goldbaum, M. (2000). Locating blood vessels in retinal images by piecewise threshold probing of a matched filter response. *IEEE Transactions on Medical Imaging*, *19*, 203–210 March.
9. Chaudhuri, S., Chatterjee, S., Katz, N., Nelson, M., & Goldbaum, M. (1989). Detection of blood vessels in retinal images using two-dimensional matched filters. *IEEE Transactions on Medical Imaging*, *8*(3), 263–269.
10. Martínez-Pérez, M. E., Hughes, A. D., Stanton, A. V., Thom, S. A., Bharath, A. A., & Parker, K. H. (1999). Retinal blood vessel segmentation by means of scale-space analysis and region growing. In *Medical Image Computing and Computer-assisted Intervention—MICCAI*, 90–97.
11. Gang, L., Chutatape, O., & Krishnan, S. M. (2002). Detection and measurement of retinal vessels in fundus images using amplitude modified second-order Gaussian filter. *IEEE Transactions on Biomedical Engineering*, *49*(2), 168–172.
12. Jiang, X., & Mojon, D. (2003). Adaptive local thresholding by verification-based multithreshold probing with application to vessel detection in retinal images. *IEEE Transactions on Pattern Analysis and Machine Intelligence*, *25*(1), 131–137.
13. Soares, J. V. B., Leandro, J. J. G., Cesar Jr., R. M., Jelinek, H. F., & Cree, M. J. (2006). Retinal vessel segmentation using the 2-D Gabor wavelet and supervised classification. *IEEE Transactions on Medical Imaging*, *25*, 1214–1222.
14. Zana, F., & Klein, J. -C. (2001). Segmentation of vessel-like patterns using mathematical morphology and curvature evaluation. *IEEE Transactions on Medical Imaging*, *11*(7), 1111–1119.
15. Mendonca, A. M., & Campilho, A. (2006). Segmentation of retinal blood vessels by combining the detection of centrelines and morphological reconstruction. *IEEE Transactions On Medical Imaging*, *25*(9), 1200–1213.
16. Can, A., Shen, H., Turner, J. N., Tanenbaum, H. L., & Roysam, B. (1999). Rapid automated tracing and feature extraction from retinal fundus images using direct exploratory algorithms. *IEEE Transactions on Information Technology in Biomedicine*, *3*(2), 125–138.
17. Tolias, Y. A., & Panas, S. M. (1998). A fuzzy vessel tracking algorithm for retinal images based on fuzzy clustering. *IEEE Transactions on Medical Imaging*, *17*(2), 263–273.
18. Chutatape, O., Zheng, L., & Krishnan, S. M. (1998). Retinal blood vessel detection and tracking by matched Gaussian and Kalman filters. In *Proc. of the 20th Annual International Conference of the IEEE Engineering in Medicine and Biology Society (EMBS'98)*, *20*, 3144–3149.
19. Gao, X., Bharath, A., Stanton, A., Hughes, A., Chapman, N., & Thom, S. (2001). A method of vessel tracking for vessel diameter measurement on retinal images. In *ICIP01*, II, 881–884.
20. Sinthanayothin, C., Boyce, J., & Williamson, C. T. (1999). Automated localisation of the optic disc, fovea, and retinal blood vessels from digital colour fundus images. *British Journal of Ophthalmology*, *83*, 902–910.
21. Staal, J. J., Abramoff, M. D., Niemeijer, M., Viergever, M. A., & van Ginneken, B. (2004). Ridge based vessel segmentation in color images of the retina. *IEEE Transactions on Medical Imaging*, *23*(4), 501–509.
22. Rudin, L., Osher, S., & Fatemi, E. (1992). Nonlinear total variation based noise removal algorithms. *Physica D*, *60*, 259–268.
23. Vese, L., & Osher, S. (2003). Modeling textures with total variation minimization and oscillating patterns in image processing. *Journal Scientific Computing*, *9*, 553–572.
24. Chambolle, A. (2004). “An algorithm for total variation minimization and applications. *Journal Mathematical Imaging and Vision*, *20*, 89–97.
25. Aujol, J. F., Aubert, G., Blanc-Féraud, L., & Chambolle, A. (2005). Image decomposition into a bounded variation component and an oscillating component. *Journal of Mathematical Imaging and Vision*, *22*(1), 71–88.
26. Meyer, Y. (2001). *Oscillating patterns in image processing and in some nonlinear evolution equations*. The Fifteenth Dean Jacqueline B. Lewis Memorial Lectures. AMS:Boston MA, USA.
27. Strong, D., & Chan, T. (2003). Edge-preserving and scale-dependent properties of total variation regularization. *Inverse Problems*, *19*(6), 165–187.
28. Strong, D., Aujol, J.-F., & Chan, T. (2006). Scale recognition, regularization parameter selection, and Meyer's G norm in total variation regularization. *SIAM Journal on Multiscale Modeling and Simulation*, *5*(1), 273–303.
29. Aujol, J. F., Gilboa, G., Chan, T., & Osher, S. (2006). Structure-texture image decomposition—Modeling, algorithms, and parameter selection. *International Journal of Computer Vision*, *67*(1), 111–136.
30. Gilboa, G., Sochen, N., & Zeevi, Y. Y. (2006). Estimation of optimal PDE-based denoising in the SNR sense. *IEEE Transactions on Image Processing*, *15*(8), 2269–2280.
31. Aujol, J.-F., & Chambolle, A. (2005). Dual norms and image decomposition models. *International Journal of Computer Vision*, *63*(1), 85–104.
32. Tong, C. S., Zhang, Y., & Zheng, N. (2005). Variational image binarization and its multiscale realizations. *Journal of Mathematical Imaging and Vision*, *23*, 185–198.

Yongping Zhang was born in Shaanxi, China, in 1963. He received a Master degree of Science from Shaanxi Normal University, China in 1988 and a Ph.D. from Xi’an Jiaotong University, China in 1998. From 1999 to 2001, he was with Xi’an Jiaotong University, Xi’an, China, where he was Associate Professor. From 2001 to 2003, he was with Massey University, Palmerston North, New Zealand, where he was Postdoctoral Fellow. From 2003 to 2005, he was with Auckland UniServices Limited and Bioengineering Institute at The University of Auckland, New Zealand, where he was Research Scientist. From 2006 to 2007, he was with National University of Singapore, Singapore, where he was Research Fellow. Since the fall of 2007, he has been with Ningbo University of Technology, Ningbo, China, where he is full Professor in Bioengineering. His research interests focus on Medical image processing, Bioengineering, Computer vision and Pattern recognition.

Wynne Hsu is an Associate Professor at the Department of Computer Science and Vice Dean (Graduate Studies), School of Computing, National University of Singapore (NUS). She received her B.Sc. in computer science at National University of Singapore and her M.Sc. and Ph.D. in electrical engineering from Purdue University, West Lafayette, USA, in 1989 and 1994, respectively. She has published more than 100 technical research papers in various international journals, conference proceedings, and books. She has also served as a program committee member in numerous international conferences including VLDB, IEEE ICDE, SIGKDD, PAKDD, and DASFAA. Dr. Hsu is the principal investigator of a number of government-funded research projects. Her research interests include: knowledge discovery in databases with emphasis on data mining algorithms in relational databases, XML databases, image databases, and spatio-temporal databases.

Mong Li Lee is an Associate Professor and Assistant Dean (Undergraduate Studies) in the School of Computing at the National University of Singapore. She received her Ph.D., M.Sc. and B.Sc. (Hons 1) degrees in Computer Science from the National University of Singapore in 1999, 1992 and 1989 respectively. She was awarded the IEEE Singapore Information Technology Gold Medal for being the top student in the Computer Science program in 1989. Mong Li joined the Department of Computer Science, National University of Singapore, as a Senior Tutor in April 1989 and was appointed Fellow in the School of Computing in February 1999. Her research interests include the cleaning and integration of heterogeneous and semi-structured data, database performance issues in dynamic environments, and medical informatics.